Solid State Ionics 301 (2017) 1–9

Contents lists available at ScienceDirect

Solid State Ionics

journal homepage: www.elsevier.com/locate/ssi

A new NASICON lithium ion-conducting glass-ceramic of the $Li_{1+x}Cr_x(Ge_yTi_{1-y})_{2-x}(PO_4)_3$ system

Rafael Bianchini Nuernberg *, Ana Candida Martins Rodrigues

Laboratório de Materiais Vítreos-LaMaV, Departamento de Engenharia de Materiais, Universidade Federal de São Carlos, Rod. Washington Luiz, km 235, 13565-905, São Carlos, SP, Brazil

ARTICLE INFO

Article history:
Received 22 October 2016
Received in revised form 6 January 2017
Accepted 7 January 2017
Available online xxxx

Keywords:
Lithium ion-conductor
NASICON structure
Crystallization, glass-ceramic
$Li_{1+x}Cr_x(Ge_yTi_{1-y})_{2-x}(PO_4)_3$ system

ABSTRACT

We propose a new lithium ion-conducting glass-ceramic based on the $Li_{1+x}Cr_x(Ge_yTi_{1-y})_{2-x}(PO_4)_3$ (LCGTP) system. A specific composition ($x = y = 0.4$) of this system was synthesized by the melt-quenching method, followed by crystallization. The crystallization behavior of the precursor glass was examined by differential scanning calorimetry(DSC) and infrared spectroscopy (IR). The main results indicate that the LCGTP precursor glass presents homogeneous nucleation and considerable glass stability, which allows solid electrolytes to be obtained by the glass-ceramic route. After heat treatment, this glass crystallizes in a NASICON $LiTi_2(PO_4)_3$-type phase, demonstrating that the proposed system can accommodate Cr, Ti and Ge in an octahedral site. Different heat treatment temperatures were employed to obtain these glass-ceramics. Ionic conductivity was measured by electrochemical impedance spectroscopy (EIS). The sample heat-treated at 900 °C for 12 h showed the highest ionic conductivity at room temperature ($6.6 \times 10^{-5}\Omega^{-1}\ cm^{-1}$). This specific glass-ceramic presented a remarkably low activation energy (0.274 eV) related to grain contribution, which culminated in a grain conductivity of $8.5 \times 10^{-4}\Omega^{-1}\ cm^{-1}$ at room temperature. In addition, a correlation was found between the cell volume and the activation energy for lithium conduction. The samples' microstructures were examined by scanning electron microscopy (SEM) and were also correlated to their ionic conductivity. This set of results suggests that the proposed system is promising for the development of fast lithium ion-conducting glass-ceramics with further compositional optimization.

1. Introduction

Li-ion batteries have an unexcelled combination of high energy and power density, making this the technology of choice for portable electronics, power tools, electric vehicles and large-scale energy storage systems for intermittent power generation. Battery performance depends critically on the materials used, and a challenge is the development of safer and more reliable electrolytes. In this respect, inorganic solid lithium ion conductors present potential advantages, such as the absence of leakage and pollution, negligible electronic conductivity and high electrochemical and thermal stability [1,2,3,4,5,6]. Among the main lithium ion conductors are the NASICON-type structured phosphates [7,8,9,10]. The general formula of a NASICON-type compound is $LiM_2(PO_4)_3$, where M is a tetravalent cation (Ge, Ti, Zr, Sn or Hf). Thus, the NASICON structure consists of a covalent skeleton containing an MO_6 octahedron connected by corners to a PO_4 tetrahedron, forming 3D interconnected channels that enable conductor cations to move through the structure with low activation energy. Therefore, the structural and electrical properties of NASICON-type compounds depend on the composition of the framework [4,5,7,11]. Conductivity measurements through NASICON-type lithium phosphates with M cations of different sizes under octahedral coordination (Ge < Ti < Sn < Zr < Hf) revealed that the activation energy for ion conduction is minimal at a cell volume of 1.310 nm^3, which was achieved with titanium (Ti) in the $LiTi_2(PO_4)_3$ (LTP) system [5,11]. Additionally, the partial substitution of the M^{+4} cation by a trivalent cation, A^{+3} (Al, Ga, In, Sc, Y, La, Cr, Fe, etc.), generates a deficiency in positive charge, which is compensated by additional Li^+ ions, leading to the general $Li_{1+x}A_xM_{2-x}(PO_4)_3$ system and to enhanced conductivity [12,13]. Therefore, one of the main advantages of NASICON-type lithium ion conductors is their compositional versatility, since the NASICON structure accepts a wide range of different compositions while maintaining its structural integrity.

Thanks to their aforementioned characteristics, numerous chemical compositions of NASICON electrolytes have been successfully synthesized using different synthesis routes, such as sol-gel [14,15,16], solid state reaction [12,13,17] and glass-ceramic route [8,18,19]. In this respect, the glass-ceramic route offers clear advantages over any route that requires a further sintering stage to consolidate the electrolyte. This route allows one to obtain a pore free electrolyte and to design its microstructure by controlling glass crystallization [8,18,20]. On the other hand, the main drawback of the glass-ceramic route is the fact

* Corresponding author.
E-mail address: Rafael_nuernberg@ppgcem.ufscar.br (R.B. Nuernberg).

http://dx.doi.org/10.1016/j.ssi.2017.01.004
0167-2738/

that not all NASICON compositions can form a glass at the typical cooling rates used in the laboratory or industrial scale. In fact, only a few oxides (B_2O_3, SiO_2, P_2O_5, GeO_2) are known to form glass easily, and they must be present in a molar ratio of about 50% [21,22]. Moreover, to properly control glass crystallization, the parent glass must nucleate homogeneously [8,18].

Based on these concepts, this paper introduces a new series of NASICON compositions based on the $Li_{1+x}Cr_x(Ge_yTi_{1-y})_{2-x}(PO_4)_3$ system. Previous investigations focused on the substitution of titanium (Ti) with chromium (Cr) based on the $Li_{1+x}Cr_xTi_{2-x}(PO_4)_3$ (LCTP) system, with ceramic powders consolidated by the sintering route, resulting in electrolytes with up to 28% of porosity [10,12]. To reduce this porosity, one could envisage synthesis by the glass-ceramic route, which may lead to materials with reduced porosity [23]. However, the LCTP system has no appreciable glass forming ability because of its low glass former content. On the other hand, the $Li_{1+x}Cr_xGe_{2-x}(PO_4)_3$ (LCGP) system has already been synthesized by the glass-ceramic route, which leads to the formation of NASICON phase and ionic conductivities higher than 10^{-4} [19]. However, the Cr^{+3} ionic radius in octahedral coordination (0.0755 nm) is much closer to Ti^{+4} (0.0745 nm) than to Ge^{+4} (0.0670 nm) [24]. Therefore, the proposal of the $Li_{1+x}Cr_x(Ge_yTi_{1-y})_{2-x}(PO_4)_3$(LCGTP) system is based on the rationale that the introduction of GeO_2 increases the glass forming ability of the precursor glass, whereas the presence of TiO_2 will help to keep the NASICON cell parameters close to those of LTP system. To counterbalance these two requirements, a suitable compromise is needed between x and y substitution. Thus, we propose to synthesize a particular composition ($Li_{1.4}Cr_{0.4}(Ge_{0.4}Ti_{0.6})_{1.6}(PO_4)_3$) of the proposed LCGTP system by the glass-ceramic route and to investigate its glass forming ability, crystallization behavior (homogenous or heterogeneous) and formation of the NASICON-type phase as well as its electrical properties. The correlation between microstructure and ionic conductivity of glass-ceramics obtained under different heat treatment temperatures is also discussed.

2. Experimental

2.1. Glass and glass-ceramic preparation

LCGTP precursor glass was obtained by melting a mixture of reagents with a $17.5Li_2O \cdot 5Cr_2O_3 \cdot 16GeO_2 \cdot 24TiO_2 \cdot 37.5P_2O_5$ oxide molar ratio, corresponding to the stoichiometric chemical formula $Li_{1.4}Cr_{0.4}(Ge_{0.4}Ti_{0.6})_{1.6}(PO_4)_3$. Suitable amounts of Li_2CO_3 (99.0%, Synth, Brazil), Cr_2O_3 (99.0%, Aldrich, USA), GeO_2 (99.99%, Alfa Aesar, USA), TiO_2 (99.9%, Aldrich, USA) and $NH_4H_2PO_4$ (98%, Aldrich, USA) were used as raw materials. These reactants were homogenized in a roll ball mill for 12 h, using zirconia balls, and the resulting mixture was calcined in a platinum crucible on a hot plate in order to decompose $NH_4H_2PO_4$ and prevent chemical attack of the platinum crucible at higher temperatures. The resulting powder was melted at 1450 °C for 120 min and the low viscosity liquid was splat-cooled in a brass die to prevent crystallization. The quenched glass was annealed at 550 °C for 2 h to relieve thermal stresses. After cooling, the resulting glass was bubble-free, transparent, with an intense green color (see Fig. 3) probably caused by its chromium content. The LCGTP glass thus obtained was heat-treated for 12 h in the form of bulk samples at the DSC crystallization peak temperature (Tp), ~700 °C, and also at higher temperatures of 800 °C, 900 °C and 1000 °C, giving rise to samples HT700, HT800, HT900, HT1000. To investigate the crystallization behavior of the proposed glass composition, additional heat treatments of 5 min at Tp were also performed on bulk and powder samples.

2.2. Glass and glass-ceramic characterization

DSC analyses of glass samples were performed at a heating rate of 10 K min^{-1}, using a Netzsch DSC 404 differential scanning calorimeter equipped with platinum pans and covers. Powder and bulk samples were subjected to the same DSC procedure to evaluate their crystallization behavior (surface or bulk crystallization). To obtain powder samples with two different average particle sizes, small pieces of the glass were ground manually in an agate mortar until the powder passed through a 150 or 40 μm mesh sieve; these samples were dubbed P150-Glass and P40-Glass, respectively. The characteristic temperatures of the precursor glass, such as glass transition temperature (Tg), crystallization onset temperature (Tx) and crystallization peak temperature (Tp) were determined from the DSC curves. The melting temperature of the glass-ceramics could not be determined from the DSC curve because of the temperature limit of the calorimeter. Glass crystallization was monitored by optical dilatometry (OD) in a Misura M3D1600 dilatometer, also applying a heating rate of 10 K min^{-1}, and the melting temperature (Tm) of the glass-ceramic was determined.

To confirm the glassy nature of LCGTP precursor glass, an X-ray diffraction (XRD) analysis of a bulk glass sample was performed in a Rigaku Ultima IV diffractometer equipped with Cu Kα radiation, at a continuous scan speed of 0.02°/s in the 2 theta range of 5 to 90°. The same conditions of XRD analysis were employed to characterize the glass-ceramic samples heat-treated for 12 h. In addition, XRD analyses of glass-ceramic samples heat-treated for 5 min in bulk and powder form were also performed in order to examine the crystalline phases formed, based on the DSC peaks. A further structural analysis of powder and bulk samples of LCGTP glass was performed by Fourier transform infrared spectroscopy (FT-IR). All the infrared spectra were recorded at room temperature in a Perkin Elmer Spectrum-GX spectrometer operating in reflectance mode, in the wavenumber range of 4000–400 cm^{-1}, applying 30 scans and a resolution if 1 cm^{-1}. The bulk and powder glass-ceramic samples heat-treated for 5 min were also analyzed by FTIR in the same conditions. Fracture surfaces of bulk glass-ceramic samples heat-treated for 12 h were prepared for SEM analyses by breaking the samples and sputtering gold on the freshly fractured surfaces. SEM micrographs were recorded with a FEI Inspect S50 scanning electron microscope, and chemical analyses of these samples by energy dispersive X-ray spectroscopy (EDX) were performed in the same device.

2.3. Electrical characterization

The electrical conductivity of LCGTP glass and glass-ceramics heat-treated for 12 h was estimated by electrochemical impedance spectroscopy (EIS), using a Novocontrol Alpha impedance analyzer in the frequency range of 10^7–1 Hz, applying a voltage amplitude of 500 mV in a temperature range of 300–400 K. Temperature was controlled by using the Novotherm temperature control system, with a maximum temperature variation of ±0.1 K during the EIS measurements. These measurements were taken from polished samples gold-sputtered on both parallel sides to ensure electrical contact. The samples were about 0.1 cm thick and had an electrode contact area of 0.1 to 0.2 cm^2. The results were fitted by means of ZView 3.2b software, using an appropriate equivalent circuit.

3. Results

3.1. Structural characterization

To produce highly crystalline glass-ceramics, bulk glass samples were crystallized for 12 h at different temperatures. Fig. 3 illustrates the XRD results of bulk samples heat-treated at 700 °C, 800 °C, 900 °C and 1000 °C for 12 h. NASICON $LiTi_2(PO_4)_3$-type phase (JCPDS card 35-754) was crystallized in all the glass-ceramics and the intensity of the XRD pattern increased along with the heat treatment temperature (see intensity bars, Fig. 3). This behavior is well known, and has already been observed in a number of NASICON phosphate systems [18,23,25]. A small diffraction peak, which is visible in all the samples, was

attributed to a second minor phase, Li_2TiO_3 (JCPDS card 71-2348), albeit with some uncertainty since only one small peak corresponding to this phase is detectable.

3.2. Thermal characterization of LCGTP glass

Fig. 1 shows DSC analyses of samples of LCGTP precursor glass (Bulk-Glass), coarse powder (P150-Glass) and fine powder (P40-Glass). The DSC analysis of LCGTP bulk glass revealed a very intensive and narrow crystallization peak with a well-defined crystallization peak (Tp) and a glass transition (Tg) temperature. On the other hand, the DSC curves of the powder samples did not show a clear Tg, while the finest powder (P40-Glass) showed two crystallization peaks at 711 °C and 741 °C (insert of Fig. 1). Furthermore, the Tp of the glass powder samples shifted unexpectedly to a higher temperature when compared to the Tp of the bulk sample.

In addition, the melting temperature (Tm) of the crystallized phase was determined from an OD analysis. Fig. 2 shows the shrinkage area of the projected shadow of a parallelepipedal glass sample as a function of temperature. Note that two characteristic events can be observed here. The first event at 695 °C (inflection point) is a slight shrinkage of about 1% (Fig. 2, insert) in the same temperature range of Tp (699 °C) determined from the DSC analysis. Theoretically, the DSC temperature peak should match the OD temperature inflection point, since DSC measures heat flow as a response and OD measures shrinkage. Nonetheless, this difference of 4 °C is quite reasonable, despite the inherent differences between these methods and devices. Thus, this shrinkage pertains to the crystallization process and indicates that the molar density of crystallized phase is slightly higher than that of the parent glass, as expected. Slighter expansions than those that occurred before and after the crystallization event were attributed to thermal expansion of the glass and the crystal, respectively. These kinds of expansion were seen in the entire temperature range and took place in steps due to the precision limit of the equipment. The second event occurred above 1330 °C, when the sample melted. The $Li_{1.4}Cr_{0.4}(Ge_{0.4}Ti_{0.6})_{1.6}(PO_4)_3$ system is a solid solution, so the crystallized phase begins to melt at about 1330 °C and finishes melting at 1346 °C, when the entire sample is liquid (Fig. 2). The latter temperature is the *liquidus* temperature and was considered the Tm.

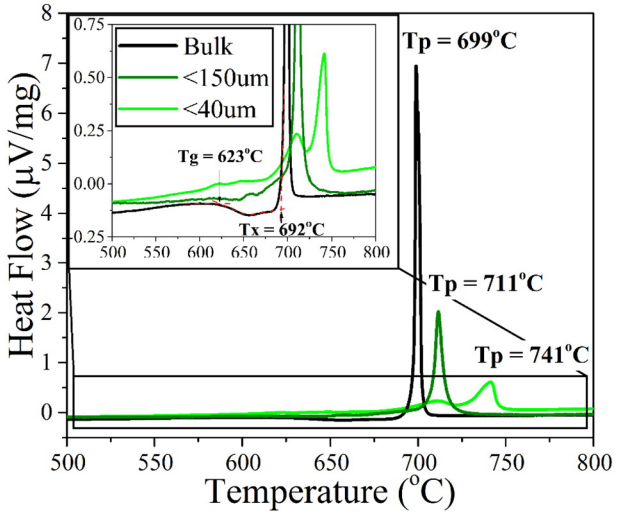

Fig. 1. DSC curves at a heating rate of 10 K min^{-1} of samples of LCGTP precursor glass (Bulk-Glass), coarse (P150-Glass) and fine (P40-Glass) powder. The crystallization peak temperatures, Tp, are indicated for all samples, while Tx and Tg are indicated only for the bulk glass sample.

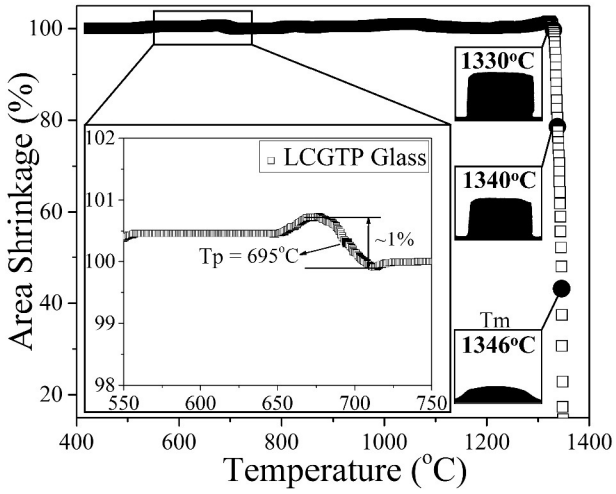

Fig. 2. Optical dilatometry data at a heating rate of 10 K min^{-1} for a parallelepiped sample of LCGTP glass. Tp and Tm, as well as some photographs from the OD analysis, are included in the plot.

3.3. Electrical characterization

The EIS data of the LCGTP glass and glass-ceramics revealed typical ion-conductive behavior. In fact, the complex impedance plot shows a spike of points at low frequency resulting from the effect of ionic polarization [8,18,19,26]. Fig. 4 presents impedance data obtained at room temperature (300*K*) for the glass-ceramic samples HT700, HT800 and HT900. Three distinct contributions can be noted: a spike in the low-frequency range (Fig. 4, left) ascribed to polarization of the electrode due to lithium ions blocked by the metallic (Au) electrode; a depressed semi-circle in the intermediate frequency range, corresponding to grain boundary resistance (Fig. 4, right); and a partial semi-circle in the high-frequency range pertaining to grain resistance (Fig. 4, insert). In order to separate these different contributions, impedance data were fitted based on an equivalent circuit comprising a parallel combination of resistance (R_g) and capacitance (C_g) attributed to the grain contribution ($R_g|C_g$), in series with a parallel combination of a resistance (R_{gb}) and a constant-phase element (CPE_{gb}) attributed to the grain boundary contribution ($R_{gb}|CPE_{gb}$) and in series with a constant-phase element (CPE_e) which accounts for the electrode polarization effects in the low frequency region.

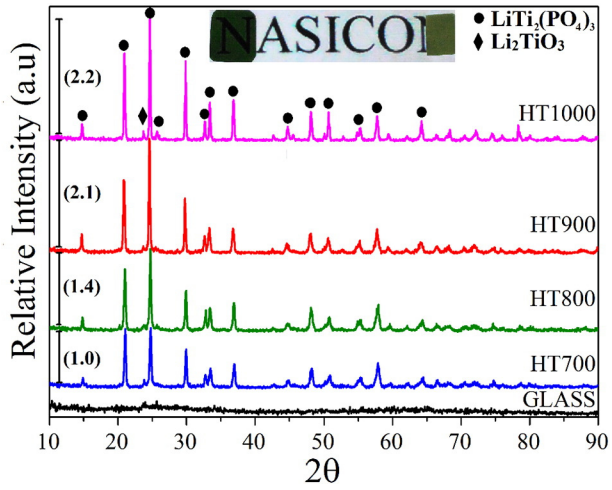

Fig. 3. XRD patterns of LCGTP bulk glass and glass-ceramics heat-treated for 12 h at 700 °C (HT700), 800 °C (HT800), 900 °C (HT900) and 1000 °C (HT1000). A cropping of a digital photograph of the LCGTP glass (left) and glass ceramic (right) is also shown.

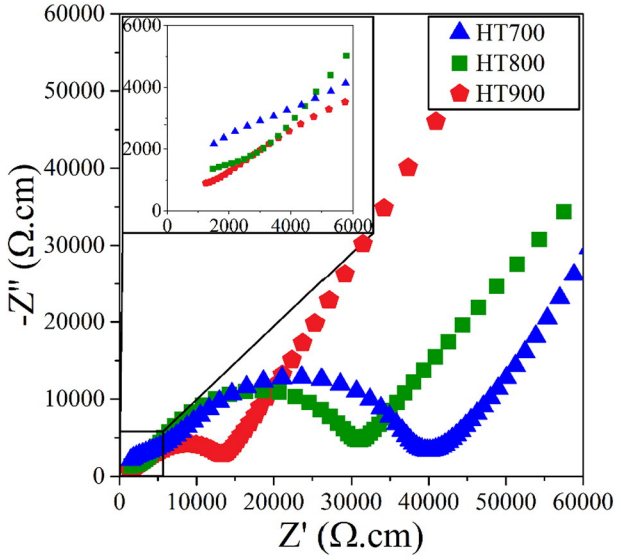

Fig. 4. Impedance data recorded at room temperature (300 K) of LCGTP glass ceramic samples HT700, HT800 and HT900. Data of LCGTP glass and HT1000 samples are not shown here due to scale compatibility.

Fig. 5 shows an example of the complex impedance plot, including experimental data and the result of fitting, as well as the equivalent circuit ($[R_g|C_g] - [R_{gb}|CPE_{gb}] - CPE_e$) used in the fitting procedure. In the case of the glass sample, the equivalent circuit has only a parallel combination of a resistance (R_a) and a constant-phase element (CPE_a) in series with a constant-phase element (CPEe) to describe the electrode polarization ($[R_a|C_a] - CPE_e$). The impedance of the constant-phase element (CPE) is given by Eq. (1), where ω is the angular frequency and Q and n pertain, respectively, to the capacitance and depression angle ($n \leq 1$) [17,26,27,28].

$$Z_{CPE} = \frac{1}{Q(i\omega)^n} \tag{1}$$

In all the glass-ceramics and in the entire temperature range, fitting results of the grain capacitance (Cg) showed values varying from 8×10^{-12} to 9×10^{-11} F, which is in agreement with the range proposed by Irvine et al. [29]. The effective capacitance (C_{gb}) of the grain boundary was determined based on Eq. (2) [17,26,27,28] and ranged from 1×10^{-10} to 2×10^{-9} F, also in agreement with Irvine et al. [29], while the fitting parameter n_{gb} was found to range from 0.6 to 0.9. The electrode capacitance of the fitted data in Fig. 5 was found to be 5.3×10^{-6}F. A rough estimation, considering a monolayer of Li^{+1} ions with an ionic radius of 76 pm blocked on both sides of the electrode, based on the electrode area of the HT700 sample (0.167 cm^2) and a reasonable ε_r of 2, results in a capacitance of 1.9×10^{-6}F. Thus, all the fitting results were reasonable for the polycrystalline ionic conductor class [29], suggesting that the equivalent circuit used here can properly describe the electrolytes investigated in this study.

$$C_{gb} = \frac{(R_{gb}Q_{gb})^{\frac{1}{n_{gb}}}}{R_{gb}} \tag{2}$$

The total ionic conductivity (σ_t) of the glass-ceramics was determined by applying Eq. (3) [17,26] to the grain (R_g) and grain boundary (R_{gb}) resistances obtained by the fitting procedure. Here, t denotes the sample's thickness and S the area of the electrode in contact with the sample.

$$\sigma_t = \frac{1}{R_g + R_{gb}} \cdot \frac{t}{S} \tag{3}$$

The dependence of total ionic conductivity on the inverse of temperature was plotted following the Arrhenius relation expressed in Eq. (4) [19,26], where k_b is Boltzmann's constant, T is the absolute temperature, A is the pre-exponential factor and Ea is the activation energy for ion conduction.

$$\sigma T = A\exp\left(\frac{-E_a}{k_b T}\right) \tag{4}$$

Fig. 6 shows the Arrhenius plot of total ionic conductivity (σ_t) for glass-ceramics obtained at different temperatures, together with the ionic conductivity of the LCGTP precursor glass. The ionic conductivity of glass-ceramics is up to 5 orders of magnitude higher than that of the parent glass. This result demonstrates how specific the NASICON structure is, since the conductivity of a glass is usually higher than that of its isochemical crystal [11]. In addition, the glass-ceramics obtained with a single heat treatment at 900 °C (HT900) showed the highest

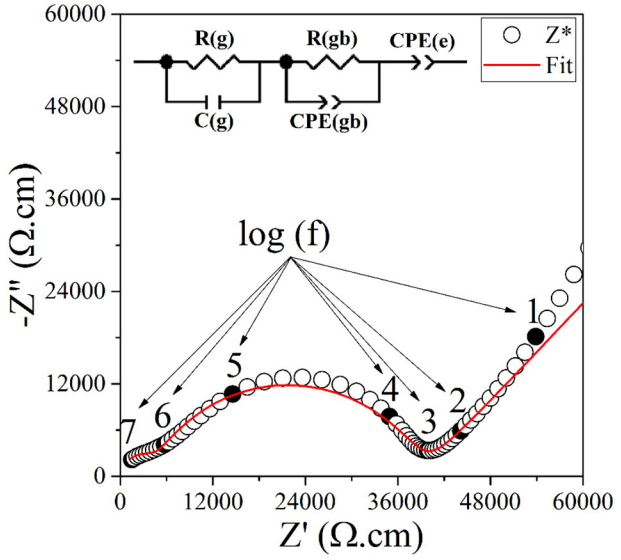

Fig. 5. Complex impedance plot for sample HT700 recorded at room temperature (300 K). Symbols represent the experimental data and the line indicates the result of fitting based on the equivalent circuit shown here.

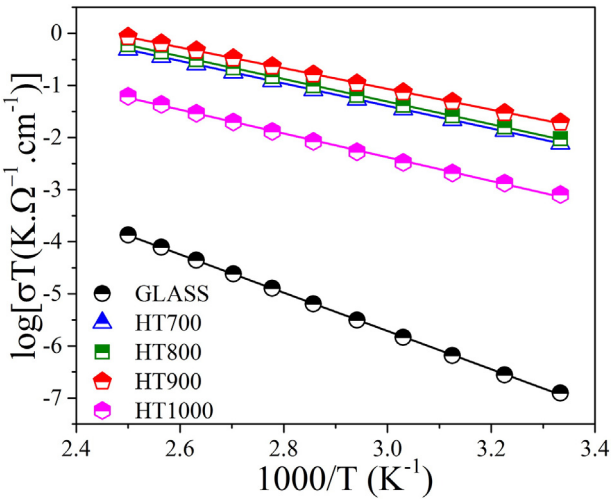

Fig. 6. Arrhenius plot of total ionic conductivity of the LCGTP glass-ceramics heat-treated at 700 °C (HT700), 800 °C (HT800), 900 °C (HT900) and 1000 °C (HT1000). The ionic conductivity of the precursor glass is also shown.

total conductivity in the entire temperature range ($6.6 \times 10^{-5}\Omega^{-1}$ cm^{-1} at 300 K).

The activation energy for ion conduction in LCGTP glass and glass-ceramics was calculated by linear regression of the experimental points shown in Fig. 6. Table 2 summarizes the total ionic conductivity at room temperature (300 K), as well as the related activation energy and the logarithm of the pre-exponential term of Eq. (4), log(A). Comparing the results related to total contribution of LCGTP glass and glass-ceramics (Table 2), it is clear that the main difference between them lies in the activation energy, since the values of log(A) in glass and glass-ceramics are comparable.

3.4. Microstructural characterization

Fig. 7 shows SEM micrographs of fracture surface of the glass-ceramics at different levels of magnification. Samples HT700 and HT800 show irregular fracture surfaces with underdeveloped grains smaller than 1 μm of undefined shape. On the other hand, samples HT900 and HT1000 show typical NASICON cubic-shaped grains [14,17,19,26] larger than 1 μm. Moreover, sample HT1000 shows a very regular microstructure typical of intergranular fracture. The SEM micrograph of sample HT1000 also shows spherical grains, indicated by arrows, which were evaluated by the EDX chemical analysis. In summary, these results also confirm the prevalence of internal crystallization in the LCGTP glass, since surface-crystallized glass-ceramics normally show textured microstructures with elongated grains grown from surface. It is also possible to note the low porosity of the glass-ceramic samples in Fig. 7. The low porosity of HT900 sample was confirmed by a rough estimation using the apparent and the theoretical density of this sample. Its apparent density (2.98 g/cm^3) was estimated by using the sample's dimensions and mass. On the other hand, the theoretical density (3.14 g/cm^3) was calculated considering six formula units, as suggested by Hagman and Kierkegaard [30] and the nominal molar mass (407.9 g/mol) of the studied composition. The unit cell volume of the sample HT900 was calculated using the lattice parameters determined from XRD analysis. It is true that this estimated value of density does not consider the residual glassy phase or other secondary phases. Even though, this estimation leads to a relative density of 95% for the HT900 sample, which is in good agreement with SEM micrograph shown in Fig. 7

The chemical composition of all the glass-ceramics was examined by EDX under 1,000× magnification (area of about 0.1 mm^2) in three different regions of the samples. Table 1 shows the average results and their respective standard errors. Lithium is not detectable in chemical characterizations by EDX, so our calculations were based on its nominal composition. Given that glass-ceramics derive from the same glass, they should have the same chemical composition. Deviations between samples were lower than 5% in every case and for all the oxides and lower than 3% between samples and their nominal chemical compositions. The chemical composition of spherical and cubic grains which were revealed under 100,000× magnification in sample HT1000 was also determined by EDX. The spherical grains were found to contain about 20 mol% of silicon, which was not found in any of the other analyses. This impurity was probably introduced by the chemical reactants used to synthesize the parent glass, since there was no contact with silicon sources in any other step of the synthesis process.

4. Discussion

4.1. Crystallization behavior

The reduced glass transition parameter (Tgr = Tg/Tm, temperatures in K) was calculated based on the Tg taken from the DSC curve and the Tm from the OD results. In this case, Tgr was found to be lower than 0.6

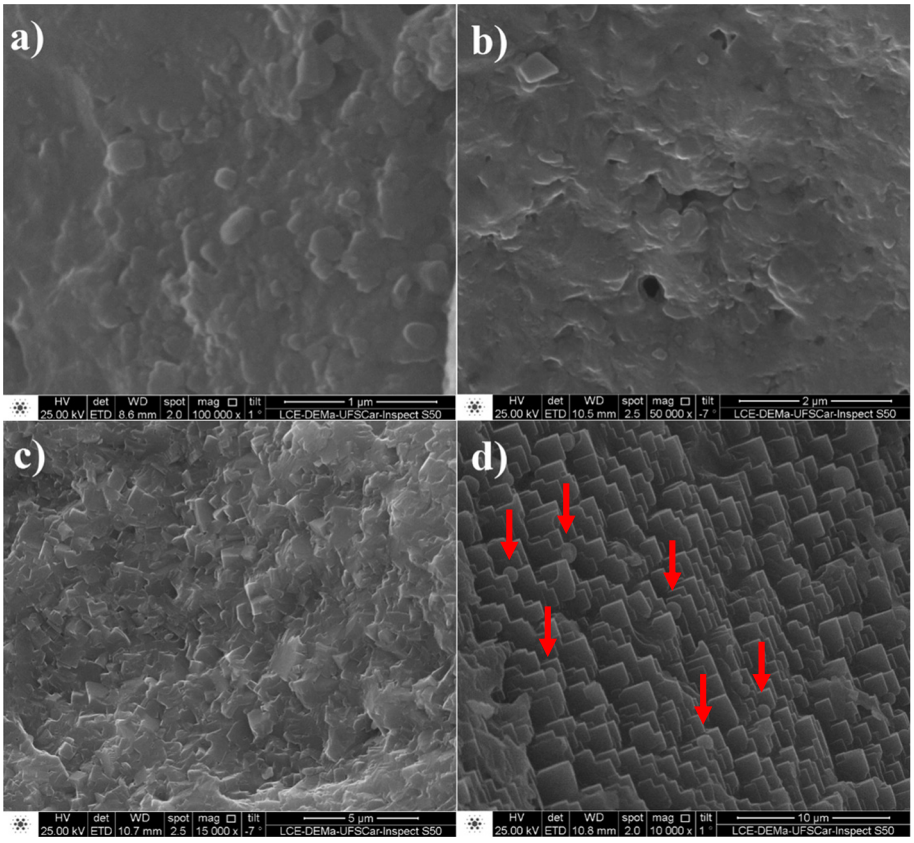

Fig. 7. SEM micrographs of surface fractures of LCGTP glass-ceramics under different levels of magnification: 100,000× for HT700 (a), 50,000× for HT800 (b), 15,000× for HT900 (c) and 10,000× for HT1000 (d). The arrows indicate a distinct grain morphology.

Table 1
EDX chemical analysis of the glass-ceramics examined in this study, and local EDX chemical analysis of different grain shapes in sample HT1000.

Oxides	Nominal (mol%)	HT700 (mol%)	HT800 (mol%)	HT900 (mol%)	HT1000 (mol%)	HT1000 Cubic (mol%)	HT1000 Spherical (mol%)
Cr_2O_3	5.0	4.8 (1)	5.9(2)	5.04(5)	4.53(8)	4.2%	2.9%
GeO_2	16.0%	16.7(2)	17.2(5)	17.1(5)	18.9(5)	16.0%	13.5%
TiO_2	24.0%	23.0(7)	26.3(5)	23.1(4)	23.7(9)	21.2%	15.1%
P_2O_5	37.5%	39.9(4)	35.1(3)	39.3(5)	37.4(3)	42.4%	32.4%
SiO_2	0.0%	–	–	–	–	0.7%	20.7%

(Tgr = 0.553), which is a strong indication that the glass under study presented homogenous nucleation [31]. The Hrüby parameter (K_H = Tx − Tg/Tm − Tx)) [32], which provides information about the stability against crystallization of a particular glass during heating [33,34], was also calculated. Furthermore, a correlation between glass stability and glass forming ability has already been established, especially in the case of the K_H parameter [33]. Thus, a higher K_H value also indicates better glass forming ability. The K_H value of the LCGTP glass of this study (K_H = 0.105) is comparable to that of well-known homogeneous nucleating glass systems such as fresnoite (0.14) [35], lithium germanium phosphate (0.11) [8] and lithium diborate (0.096) [33].

The crystallization peak temperature, Tp, should not change in bulk and powder samples when the glass shows volumetric nucleation. Conversely, if the glass shows surface crystallization due to an increase in surface area, the Tp of glass powder should shift to lower temperatures and the crystallization peak should be even narrower than that of the bulk glass sample. As can be seen in Fig. 1, the opposite behavior occurred, with Tp shifting to higher temperatures and becoming broader as the glass powder became finer. Therefore, because the Tp of the powder samples did not shift to lower temperatures, these results offer a second evidence that LCGTP glass presents bulk crystallization. In addition, these results also suggest that the larger surface area in this glass system hinders crystallization. To discover why a larger surface area impairs crystallization, we used IR analyses in reflectance mode, since this mode provides a primarily surface response. Thus, bulk and powder samples of LCGTP glass were previously heat-treated for 5 min at temperatures very close to the peak temperatures, i.e., 700 and 710 °C for bulk and coarse powder, respectively. The fine powder was heat-treated at 710 °C and 740 °C because this sample showed two distinguishable crystallization peaks on the DSC curve (Fig. 1). Fig. 8 depicts FT-IR analyses of bulk glass and glass powder before and after heat treatment.

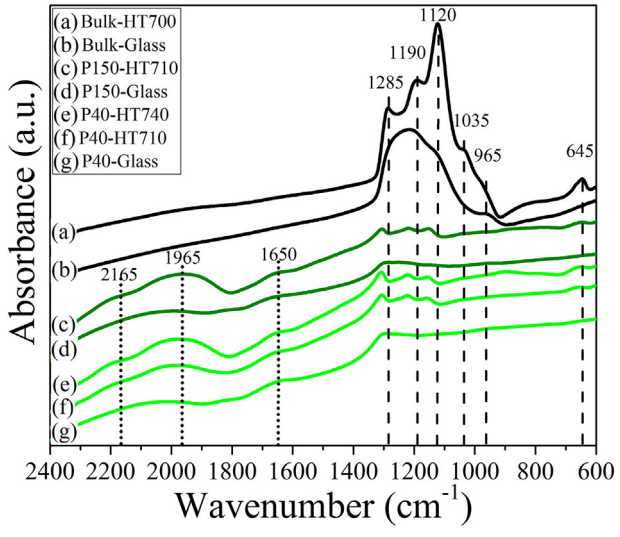

Fig. 8. FT-IR analyses of glass bulk and powder, before and after a 5 min heat treatment at a temperature close to Tp: (a) bulk glass heat-treated at 700 °C (HT700), (b) precursor glass as quenched (Bulk-Glass), (c) coarse powder heat-treated at 710 °C (P150-HT710), (d) coarse glass powder (P150-Glass), (e) fine glass powder heat-treated at 740 °C (P40-HT740), (f) fine glass powder heat-treated at 710 °C (P40-HT710), and (g) fine glass powder (P40-Glass).

The bands at 2165 and 1640 cm^{-1} marked on the dotted line appear only in powder samples (Fig .8 c, d, e, f and g) and have been assigned to a combination of vibrational modes of the P—OH bond in phosphate glasses [36,37]. These results strongly indicate that the presence of OH groups may be the reason why larger surface areas hinder the crystallization of powder samples. These OH groups are bonded to phosphorus atoms from the glass network on the particle surface and may have been introduced in the powder samples through exposure of particle surfaces to atmosphere during the grinding process. On the other hand, the bands marked by dashed lines, which are more distinguishable in heat-treated samples (Fig. 8 a, c, e, and f), have been ascribed to PO_4/MO_6 interaction (1280 cm^{-1}), PO_4 (1185 cm^{-1}, 1025 cm^{-1}, 1120 cm^{-1} and 955 cm^{-1}), and MO_6 (640 cm^{-1}) vibrational modes in NASICON type phosphates [38,39].

To characterize the crystalline phases in the heat-treated bulk, coarse and fine powder, these samples were subjected to XRD analyses, as shown in Fig. 9.

The NASICON $LiTi_2(PO_4)_3$-type phase (JCPDS card 35-754) is formed in every case, whether the sample is crystallized from powder or from bulk form, and regardless of the heat treatment temperature employed. These results provide clear evidence that the two crystallization peaks detected through the DSC analysis (Fig. 1) in fine powder pertain to different crystallization mechanisms rather than to the formation of different phases. The secondary phase, Li_2TiO_3 (JCPDS card 71-2348), was detected here as well as in the samples heat-treated for 12 h (Fig. 3). In addition, the intensity of the XRD pattern increased as the heat treatment temperature increased. On the other hand, the XRD pattern of the finest powder (P40-HT710) is less intense than that of the coarse powder (P150-HT710) when treated at same temperature (710 °C), again suggesting that the specific surface area does in fact hinder crystallization in the LCGTP glass system. The bulk glass shows less intense peaks, probably because of the lower heat treatment temperature applied.

4.2. Structural analysis

The XRD pattern of $Li_{1.4}Cr_{0.4}(Ge_{0.4}Ti_{0.6})_{1.6}(PO_4)_3$ glass-ceramics obtained after heat treatment of the precursor glass for 12 h at 700, 800, 900 and 1000 °C matches that of the NASICON $LiTi_2(PO_4)_3$-type phase (Fig. 3). In addition, the most intense peaks in the XRD pattern shift toward lower 2 theta angles as a function of heat treatment temperature,

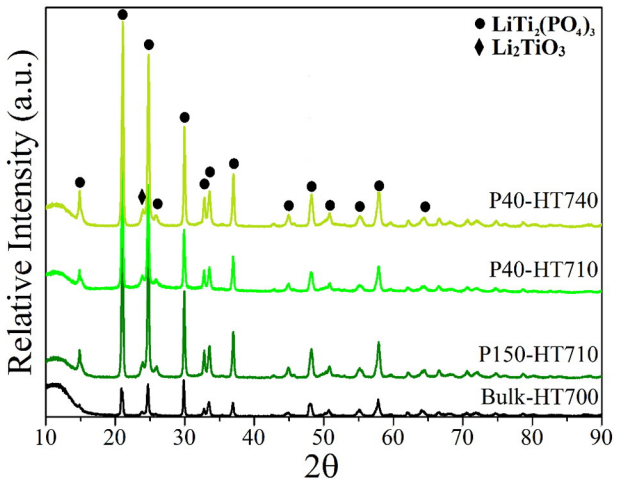

Fig. 9. XRD patterns of LCGTP glass heat-treated for 5 min as bulk sample at 700 °C (Bulk-HT700), as coarse powder at 710 °C (P150-HT710), and as fine powder at 710 °C (P40-HT710) and 740 °C (P40-HT740).

which means that the lattice parameters of the NASICON structure increase along with increasing heat treatment temperature. As the NASICON $LiTi_2(PO_4)_3$-type structure has a rhombohedral lattice (space group R-3C, trigonal system), its lattice parameters can also be represented on hexagonal axes [40]. Thus, the lattice parameters and the volume of NASICON unit cell were estimated based on the diffraction angle of the most intense peaks (planes [104] and [113]) through Eqs. (5) and (6), respectively.

$$\frac{1}{d^2} = \frac{4}{3}\left(\frac{h^2 + hk + k^2}{a^2}\right) + \frac{l^2}{c^2} \quad (5)$$

$$V = \frac{\sqrt{3}a^2 c}{2} \quad (6)$$

Fig. 10 shows the dependence of the lattice parameters (a and c) and volume of the NASICON structure on the heat treatment temperature. As can be clearly seen, the NASICON unit cell volume shows practically no variation between the heat treatment at 700 °C and at 800 °C, and increases considerably in response to the heat treatment at 900 °C, but drops again slightly after the heat treatment at 1000 °C.

Since the proposed LCGTP composition leads to a solid solution, a possible explanation for this behavior is that some components in the residual glassy phase or segregated at the grain boundary were incorporated into the NASICON phase, causing structural changes in the structure of the NASICON unit cell. In the case of sample HT1000, the opposite should occur, with some oxides being expelled from the NASICON $LiTi_2(PO_4)_3$-type phase. In summary, the estimated lattice parameters for $Li_{1.4}Cr_{0.4}(Ge_{0.4}Ti_{0.6})_{1.6}(PO_4)_3$ glass-ceramics are slightly lower than that of $LiTi_2(PO_4)_3$ (a = 0.851 and c = 2.088), JCPDS card 35-754, and higher than the lattice parameters (a = 0.829 and c = 2.053) found by Xu [19] in $Li_{1.4}Cr_{0.4}Ge_{1.6}(PO_4)_3$ glass-ceramics. Sample HT900 presented lattice parameters (a = 0.846 and c = 2.085) very close to those of $LiTi_2(PO_4)_3$. These results are in perfect agreement with our previous prediction that, the proposed $Li_{1+x}Cr_x(Ge_yTi_{1-y})_{2-x}(PO_4)_3$ system can indeed result in lattice parameters comparable to those of $LiTi_2(PO_4)_3$ through compositional tailoring.

4.3. Contribution of grain and grain boundary conductivities

In the case of glass-ceramics, it was also possible to separate the contributions of the grain and the grain boundary. As a matter of fact, since the geometrical factor (t/S) of grains and grain boundaries is unknown, only their apparent contribution can be estimated based on the geometrical factor of the whole sample. Thus, the apparent contributions of grains and grain boundaries were also calculated using Eq. (3), but

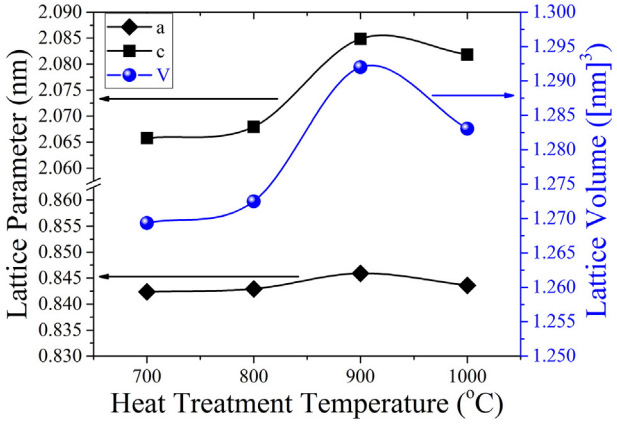

Fig. 10. Dependence of the lattice parameters (a and c) and lattice volume of the NASICON structure on heat treatment temperatures.

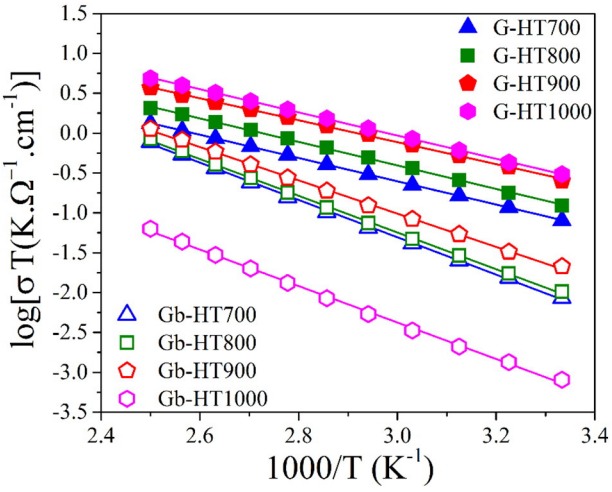

Fig. 11. Arrhenius plot of grain (closed symbols) and grain boundary (open symbols) apparent ionic conductivity as a function of inverse temperature in LCGTP glass-ceramics heat-treated at the indicated temperatures.

now, using the R_g and R_{gb} data obtained separately [17,26,27]. Fig. 11 shows an Arrhenius plot of the grain and grain boundary apparent contribution of ionic conductivity obtained at different temperatures.

Values of σ_{300K}, Ea and log(A) related to the apparent contribution of grains and grain boundaries in the synthesized glass-ceramic are also summarized in Table 2. A notably high grain conductivity of $1 \times 10^{-3}\Omega^{-1}$ cm^{-1} at room temperature was found for the glass-ceramic HT1000. The activation energy of grain conductivity decreases as a function of heat treatment temperature, except in sample HT1000. Thus, the glass-ceramic HT900 showed the lowest Ea (0.274(3) eV) related to grain contribution, which also led to high grain conductivity ($8.5 \times 10^{-4}\Omega^{-1}$ cm^{-1}) at room temperature. It is also interesting to note that grain boundaries have lower apparent conductivity (300 K) and higher activation energy than grains. The lower conductivity can be predicted from the impedance plots, Figs. 4 and 5, which show much larger semicircles due to grain boundary resistivity in comparison to that attributed to the grain contribution, at high frequencies. This also indicates that the grain boundary limits the total ionic conductivity in these glass-ceramics. In addition, the grain boundary activation energy tends to decrease with heat treatment temperature, except in the sample heat-treated at 1000 °C, indicating that increased heat treatment temperature also has a beneficial effect on the grain boundary contribution, up to 900 °C.

The results in Table 2 indicate that the activation energy of grains are the same, within experimental errors, in samples heat-treated at 700 and 800 °C, with a minimum in the sample heat-treated at 900 °C, and then, increases again in the sample heat-treated at 1000 °C. This trend may be correlated to the variation of the lattice volume, Fig. 10, which exhibits a maximum in the sample heat-treated at 900 °C. Thus, sample HT900 presented both the maximum volume lattice and the minimum activation energy related to grain ionic conductivity. The relationship between lattice volume and activation energy for ion conduction is already established in the literature [5,19,25]. However, we found no reports relating the dependence of Ea on grain contribution to the NASICON volume lattice caused by different heat treatments. With respect to grain boundary contribution, Ea follows the same trend as grain contribution. Nonetheless, the main finding about the grain boundary contribution was the log(A) term for sample HT1000, which dropped by about one order of magnitude compared to the other glass-ceramics. This was probably the main reason why sample HT1000 exhibited the lowest total ionic conductivity at room temperature (Table 2). A reasonable explanation may be a poorer contact between grains or cracks introduced in the heat treatment stage [26]. In fact, while all the glass-ceramics showed considerable mechanical

Table 2
Total ionic conductivity at room temperature (σ_{300K}), activation energy (Ea) and the pre-exponential term (log(A)) of LCGTP glass and glass-ceramics. Ionic conductivity, Ea and log[*A*] of grains and grain boundaries are also showed. The uncertainties indicated here are mathematical errors taken from the linear regression.

	Total			Grains			Grain Boundaries		
Sample	$\sigma_{300\ K}$ (S cm^{-1})	Log(A) (S cm^{-1})	Ea (eV)	$\sigma_{300\ K}$ (S cm^{-1})	Log(A) (S cm^{-1})	Ea (eV)	$\sigma_{300\ K}$ (S cm^{-1})	Log(A) (S cm^{-1})	Ea (eV)
Glass	4.2×10^{-10}	5.31(5)	0.730(3)	–	–	–	–	–	–
HT700	2.6×10^{-5}	5.09(2)	0.429(1)	2.7×10^{-4}	3.78(1)	0.290(1)	2.8×10^{-5}	5.72(5)	0.465(4)
HT800	3.2×10^{-5}	5.21(1)	0.432(1)	4.1×10^{-4}	4.02(4)	0.293(3)	3.4×10^{-5}	5.67(4)	0.458(4)
HT900	6.6×10^{-5}	4.90(3)	0.395(2)	8.5×10^{-4}	4.02(4)	0.274(3)	7.1×10^{-5}	5.26(5)	0.414(4)
HT1000	2.2×10^{-6}	4.47(4)	0.454(6)	1.0×10^{-3}	4.33(2)	0.289(1)	2.9×10^{-6}	4.49(1)	0.455(6)

strength (impossible to break manually), sample HT1000 was brittle and generally broke easily when handled. Also, the SEM analysis of sample HT1000 indicated a typical intergranular fracture, which may justify its precarious mechanical strength and may also explain the drop in grain boundary conductivity resulting from deficient contact between grains.

5. Conclusions

We proposed here a new NASICON series based on the $Li_{1+x}Cr_x(Ge_yTi_{1-y})_{2-x}(PO_4)_3$ system with a promising potential for synthesis by the glass-ceramic route. We investigated a particular composition of this system in terms of the crystallization behavior, formation of NASICON-type structure and electrical properties of the obtained glass-ceramics. The LCGTP glass under study shows internal nucleation and presents comparable thermal stability parameter to other self-nucleating glasses. Moreover, NASICON $LiTi_2(PO_4)_3$-type phase was successfully crystallized and the cell parameters of the NASICON structure were in the range of other well-known systems, indicating that the composition investigated here forms a solid solution and that the octahedral site is shared by chromium, germanium and titanium. The ionic conductivity of glass-ceramics is up to 5 orders of magnitude higher than that of the precursor glass and is dependent on the heat treatment temperature. In addition, we found a correlation between the variation of activation energy for grain contribution and variations in the NASICON lattice volume caused by different heat treatment temperatures. The highest total ionic conductivity was found in the glass-ceramic heat-treated at 900 °C, which showed a reasonable value of $6.6 \times 10^{-5}\Omega^{-1}$ cm^{-1}. The remarkably low activation energy (0.274 eV) related to grain contribution found in sample HT900 suggests that, when its microstructure is optimized, the proposed system is promising for the development of fast Li ion-conducting glass-ceramics. Further compositional adjustments could provide a compromise between glass stability (Ge addition) and the lattice parameter of the NASICON structure (addition of Ti and Cr). In fact, this stage of research is already ongoing at our research center.

Acknowledgements

The authors gratefully acknowledge the financial support of FAPESP (São Paulo Research Foundation) under CEPID process no. 2013/07793-6. R. B. Nuernberg acknowledges CNPq (Brazil's National Council for Scientific and Technological Development) for granting a doctoral scholarship under Project no. 140456/2014-7. We are also indebted to Professor Edgar Dutra Zanotto for his valuable insights on the crystallization behavior of precursor glass.

References

[1] J.W. Fergus, Ceramic and polymeric solid electrolytes for lithium-ion batteries, J. Power Sources 195 (2010) 4554–4569, http://dx.doi.org/10.1016/j.jpowsour.2010.01.076.
[2] N. Nitta, F. Wu, J.T. Lee, G. Yushin, Li-ion battery materials: present and future, Mater. Today 18 (June 2015) 252–264, http://dx.doi.org/10.1016/j.mattod.2014.10.040.
[3] S. Teng, J. Tan, A. Tiwari, Recent developments in garnet based solid state electrolytes for thin film batteries, Curr. Opinion Solid State Mater. Sci. 18 (2014) 29–38, http://dx.doi.org/10.1016/j.cossms.2013.10.002.
[4] P. Knauth, Inorganic solid Li ion conductors: an overview, Solid State Ionics 180 (2009) 911–916, http://dx.doi.org/10.1016/j.ssi.2009.03.022.
[5] K. Takada, Progress and prospective of solid-state lithium batteries, Acta Mater. 61 (2013) 759–770, http://dx.doi.org/10.1016/j.actamat.2012.10.034.
[6] Y. Zhao, Y. Ding, Y. Li, L. Peng, H.R. Byon, J.B. Goodenougha, G. Yu, A chemistry and material perspective on lithium redox flow batteries towards high-density electrical energy storage, Chem. Soc. Rev. 44 (2015) 7968–7996, http://dx.doi.org/10.1039/C5CS00289C.
[7] N. Anantharamulu, K.K. Rao, G. Rambabu, B.V. Kumar, V. Radha, A wide-ranging review on Nasicon type materials, J. Mater. Sci. 46 (2011) 2821–2837, http://dx.doi.org/10.1007/s10853-011-5302-5 (vol. 46, pp. 2821–2837, 2011).
[8] A.M. Cruz, E.B. Ferreira, A.C.M. Rodrigues, Controlled crystallization and ionic conductivity of a nanostructured LiAlGePO4 glass–ceramic, J. Non-Cryst. Solids 355 (2009) 2295–2301, http://dx.doi.org/10.1016/j.jnoncrysol.2009.07.012.
[9] B. Yan, Y. Zhu, F. Pan, J. Liu, L. Lu, Li1.5Al0.5Ge1.5(PO4)3 Li-ion conductor prepared by melt-quench and low temperature pressing, Solid State Ionics 278 (2015) 65–68, http://dx.doi.org/10.1016/j.ssi.2015.05.020.
[10] H. Aono, E. Sugimoto, Ionic conductivity and Sinterability of lithium titanium phosphate system, Solid State Ionics 40/41 (1990) 38–42, http://dx.doi.org/10.1016/0167-2738(90)90282-V.
[11] C. Cao, Z.B. Li, X.L. Wang, X.B. Zhao, W.Q. Han, Recent advances in inorganic solid electrolytes for lithium batteries, Front. Energy Res. 2 (2014) 1–10, http://dx.doi.org/10.3389/fenrg.2014.00025.
[12] H. Aono, E. Sugimoto, Y. Sadaoka, N. Imanaka, G. Adachi, Ionic conductivity of solid electrolytes based on lithium titanium phosphate, J. Electrochem. Soc. 137 (1990) 1023–1027, http://dx.doi.org/10.1149/1.2086597.
[13] H. Aono, E. Sugimoto, Y. Sadaoka, N. Imanaka, G. Adachi, Ionic conductivity of the lithium titanium phosphate $Li_{1+x}M_xTi_{2-x}(PO4)3$ (M = Al, Sc, Y, and La) systems, J. Electrochem. Soc. 136 (1989) 590–591, http://dx.doi.org/10.1149/1.2096693.
[14] X. Xu, Z. Wen, J. Wu, X. Yang, Preparation and electrical properties of NASICON-type structured Li1.4Al0.4Ti1.6(PO4)3 glass-ceramics by the citric acid-assisted sol–gel method, Solid State Ionics 178 (2007) 29–34, http://dx.doi.org/10.1016/j.ssi.2006.11.009.
[15] N.A. Mustaffa, N.S. Mohamed, Zirconium-substituted LiSn2P3O12 solid electrolytes prepared via sol-gel method, J. Sol-Gel Sci. Technol. 77 (2016) 585–593, http://dx.doi.org/10.1007/s10971-015-3886-y.
[16] P. Zhang, H. Wang, Q. Si, M. Matsui, Y. Takeda, O. Yamamoto, N. Imanishi, High lithium ion conductivity solid electrolyte of chromium and aluminum co-doped NASICON-type LiTi2(PO4)3, Solid State Ionics 272 (2015) 101–106, http://dx.doi.org/10.1016/j.ssi.2015.01.004.
[17] H. Chung, B. Kang, Increase in grain boundary ionic conductivity of Li1.5Al0.5Ge1.5(PO4)3 by adding excess lithium, Solid State Ionics 263 (2014) 125–130, http://dx.doi.org/10.1016/j.ssi.2014.05.016.
[18] J.L. Narváez-Semanate, A.C.M. Rodrigues, Microstructure and ionic conductivity of $Li_{1+x}Al_xTi_{2-x}(PO4)3$ NASICON glass-ceramics, Solid State Ionics 181 (2010) 1197–1204, http://dx.doi.org/10.1016/j.ssi.2010.05.010.
[19] X. Xu, Z. Wen, Z. Gu, X. Xu, Z. Lin, Preparation and characterization of lithium ion-conducting glass-ceramics in the $Li_{1+x}Cr_xGe_{2-x}(PO4)3$ system, Electrochem. Commun. 6 (2004) 1233–1237, http://dx.doi.org/10.1016/j.elecom.2004.09.024.
[20] E.D. Zanotto, A bright future for glass-ceramics, Am. Ceram. Soc. Bull. 89 (2010) 19–27.
[21] P.W. McMillan, The crystallization of glasses, J. Non-Cryst. Solids 52 (1982) 67–76, http://dx.doi.org/10.1016/0022-3093(82)90281-2.
[22] R.H. Doremus, Glass Science, John Wiley and Sons, New York, 1994.
[23] J. Fu, Superionic conductivity of glass-ceramics in the system Li_2O—Al_2O_3—TiO_2—P_2O_5, Solid State Ionics 96 (1997) 195–200, http://dx.doi.org/10.1016/S0167-2738(97)00018-0.
[24] R.D. Shannon, Revised effective ionic radii and systematic studies of interatomic distances in halides and Chalcogenides, Acta Crystallogr. 32 (1976) 751–767, http://dx.doi.org/10.1107/S0567739476001551.
[25] X. Xu, Z. Wen, Z. Gu, X. Xu, Z. Lin, Lithium ion conductive glass ceramics in the system $Li_{1.4}Al_{0.4}(Ge_{1-x}Ti_x)_{1.6}(PO_4)_3$ (x = 0–1), Solid State Ionics 171 (2004) 207–213, http://dx.doi.org/10.1016/j.ssi.2004.05.009.
[26] C.R. Mariappan, C. Yada, F. Rosciano, B. Roling, Correlation between micro-structural properties and ionic conductivity of $Li_{1.5}Al_{0.5}Ge_{1.5}(PO_4)_3$ ceramics, J. Power Sources 196 (2011) 6456–6464, http://dx.doi.org/10.1016/j.jpowsour.2011.03.065.
[27] C.R. Mariappan, M. Gellert, C. Yada, F. Rosciano, B. Roling, Grain boundary resistance of fast lithium ion conductors: comparison between a lithium-ion conductive

Li—Al—Ti—P—O-type glass ceramic and a $Li_{1.5}Al_{0.5}Ge_{1.5}P_3O_{12}$ ceramic, Electrochem. Commun. 14 (2012) 25–28, http://dx.doi.org/10.1016/j.elecom.2011.10.022.
[28] V.F. Lvovich, Impedance Spectroscopy: Applications to Electrochemical and Dielectric Phenomena, Wiley, Hoboken, 2012.
[29] J.T.S. Irvine, D.C. Sinclair, A.R. West, Electroceramics: characterization by impedance spectroscopy, Adv. Mater. 2 (1990) 132–138, http://dx.doi.org/10.1002/adma.19900020304.
[30] L.O. Hagman, P. Kierkegaard, The crystal structure of $NaMe_2(PO_4)_3$: Me = Ge, Ti, Zr, Acta Chem. Scand. 22 (1968) 1822–1832.
[31] E.D. Zanotto, M.C. Weinberg, Trends in homogeneous crystal nucleation in oxide glasses, Phys. Chem. Glasses 30 (1989) 186.
[32] A. Hruby, Glass stability, Czech J. Phys. B 22 (1972) 1186.
[33] M.L.F. Nascimento, L.A. Souza, E.B. Ferreira, E.D. Zanotto, Can glass stability parameters infer glass forming ability? J. Non-Cryst. Solids 351 (2005) 3296–3308, http://dx.doi.org/10.1016/j.jnoncrysol.2005.08.013.
[34] A.A. Cabral, C. Fredericci, E.D. Zanotto, A test of the Hruby parameter to estimate glass-forming ability, J. Non-Cryst. Solids 219 (1997) 182–186, http://dx.doi.org/10.1016/S0022-3093(97)00327-X.
[35] A.A. Cabral, A.A.D. Cardoso, E.D. Zanotto, Glass-forming ability versus stability of silicate glasses. I Experimental test, J. Non-Cryst. Solids 320 (2003) 1–8, http://dx.doi.org/10.1016/S0022-3093(03)00079-6.
[36] S.M. Abo-Naf, M.S. El-Amiry, A.A. Abdel-Khalek, FT-IR and UV–Vis optical absorption spectra of c-irradiated calcium phosphate glasses doped with Cr2O3, V2O5 and Fe2O3, Opt. Mater. 30 (2008) 900–909, http://dx.doi.org/10.1016/j.optmat.2007.03.013.
[37] H. Shinozaki, S. Nakashima, S. Takahashi, A. Hanada, Y. Yamamoto, Water resistance of cerium phosphate glasses as studied by in situ high temperature IR microspectroscopy, J. Non-Cryst. Solids 378 (2013) 55–60, http://dx.doi.org/10.1016/j.jnoncrysol.2013.06.016.
[38] C.J. Antony, A. Aatiq, C.Y. Panicker, M.J. Bushiri, H.T. Varghese, T.K. Manojkumar, FT-IR and FT-Raman study of Nasicon type phosphates, ASnFe(PO4)3 [a = Na2, Ca, Cd], Spectrochim. Acta A 78 (2011) 415–419, http://dx.doi.org/10.1016/j.saa.2010.11.003.
[39] A. Aatiq, M.R. Tigha, Structural and spectroscopic study of NaSbR(PO4)3 (R = Cr, Fe, in) phases, J. Mater. Charact. 28 (2013) 394–408, http://dx.doi.org/10.1017/S0885715613000882.
[40] D.E. Sands, Introduction to Crystallography, Dover Publications, New York, 1993.